Transition to weak turbulence via spatiotemporal intermittency in the Taylor-Dean system

Michael M. Degen
Department of Physics, The Ohio State University, 174 West 18th Avenue, Columbus, Ohio 43210

Innocent Mutabazi
Groupe d'Energétique et de Mécanique, Faculté des Sciences et Techniques, Université du Havre, Boîte Postale 540, F-76058 Le Havre France

C. David Andereck
Department of Physics, The Ohio State University, 174 West 18th Avenue, Columbus, Ohio 43210
(Received 31 August 1995)

The transition to weak turbulence via spatiotemporal intermittency has been studied in the Taylor-Dean system when the inner cylinder is fixed and only the outer cylinder is rotating. The spatiotemporal intermittency regime is characterized by the coexistence of laminar domains and turbulent patches for the same value of the control parameter. The transition is supercritical, but a particular boundary condition induces an imperfection. Statistical analysis of the spatiotemporal intermittency shows that the distribution of laminar domains by widths follows a power law decay near the onset, while it is exponential for higher values of the control parameter. The exponential distribution of the laminar domains has a definite threshold near which the correlation lengths and correlation times of laminar and turbulent domains diverge, reinforcing the analogy with second-order phase transitions. The exponents measured near the critical points in this experiment differ from those observed in other systems, thus showing that the spatiotemporal intermittency is not universal in character.

PACS number(s): 47.27.Cn, 47.20.Ky, 47.52.+j

I. INTRODUCTION

The phenomenon of turbulence has been and remains one of the challenging problems of nonlinear physics, even though much effort has been devoted to such an important problem with its many applications in different areas of engineering and geophysics. Recently there has been greatly renewed interest in the problem of turbulence due to the accumulated results from several problems in nonlinear physics [1], from high precision experiments [2], from computer simulations of flow turbulence, and from interesting directions of investigation such as the multifractal approach [3]. These results have given rise to promising directions of attack. (A recent review of the state of the art of turbulence studies can be found in [4].) For example, the transition to chaos in small systems involving only temporal modes has been generally understood and different scenarios have been established [5]. The transition to chaos in *extended systems* involves spatial as well as temporal degrees of freedom, which might keep or lose their spatial coherence when an external constraint is increasingly applied to the system [1,6]. There are many systems with large aspect ratio which exhibit spatiotemporal chaos, for example Rayleigh-Bénard convection in large boxes [7], the Taylor-Couette system [8], the Taylor-Dean system [9], the printer's instability [10], and the Faraday experiment [11,12], among others.

In large aspect ratio systems, a particular scenario has attracted much attention, namely so-called *spatiotemporal intermittency* or STI. This phenomenon is characterized by a space-time mixture of fluctuating spatially ordered domains and turbulent patches in the same system for a given value of the control parameter. It is often observed in boundary layer flow [13], in pipe flow [14], in plane Poiseuille flow [15,16], and in the flow between counter-rotating cylinders [8,17]. Spatiotemporal intermittency has been observed in numerical simulations of coupled map lattices [18], in nonlinear partial differential equations such as the damped Kuramoto-Sivashinsky equation [19] or the complex Ginzburg-Landau equation [20,21], and in probabilistic cellular automata [22]. In one-dimensional extended systems, spatiotemporal intermittency has been observed in experiments on Rayleigh-Bénard convection in annular geometries as well as rectangular geometries [23] at high Rayleigh numbers. The same type of transition has been reported in the printer's instability [24], in the Faraday experiment [25], and in electromagnetically forced linear vortices [26]. In most of these cases, the regime of spatiotemporal intermittency displays some features of a second-order phase transition in equilibrium systems, such as the divergence of the correlation length in the neighborhood of a threshold value that depends on the system. This striking property was pointed out by Pomeau [27], who conjectured that the transition to chaos via spatiotemporal intermittency is analogous to the process of directed percolation. In fact, above a given value of the control parameter, the turbulent bursts appearing in the space-time diagram can be associated with "active" or "contaminant" regions in the laminar ("passive" or "absorbing") background. In all the experiments reported above [23–26], the general features of the spatiotemporal intermittency, such as the spontaneous nucleation (characterized by a power law decay of the laminar domains) and the contamination (in which the laminar domains decay exponentially) have been given, but the exponents and characteristic lengths vary from one experiment to another. These results suggest that spatiotemporal inter-

mittency does not possess a universal character. Such universality might be destroyed by diverse factors such as modulation of the laminar flow pattern, or the existence of spurious additional length scales due to subtle long-range correlations in the laminar state which differ from one system to another [28].

In this paper, we report the results of an experimental investigation of the spatiotemporal intermittency observed in the Taylor-Dean system when the inner cylinder is fixed and the outer cylinder is rotating. In this configuration, with large aspect ratio, we have previously shown that the first transition is to a time-dependent traveling roll pattern, followed by a highly hysteretic bifurcation to a stationary roll pattern [29]. Upon increasing the control parameter, the stationary pattern becomes oscillatory, and an Eckhaus instability can induce spatiotemporal defects which in turn destabilize the pattern and may induce turbulent bursts. The spatiotemporal intermittency regime exists in a finite range of the control parameter before spatially homogeneous turbulence sets in. The transition to spatiotemporal intermittency is perfect when the end boundary rings are attached to the fixed inner cylinder, while it is imperfect with a definite threshold when the rings are rotating together with the outer cylinder. We confirm that whether the rings are fixed or rotate, there exists a definite threshold beyond which the STI regime displays properties similar to those of second-order phase transitions.

The paper is organized as follows: Secs. II and III describe the experimental setup and the data acquisition procedure. The results are presented in Sec. IV and their discussion in Sec. V. Section VI contains concluding remarks.

II. EXPERIMENTAL SETUP

The Taylor-Dean system has been described in detail previously [29]. It consists of two horizontal coaxial cylinders (which may rotate independently) with a partially filled gap [Fig. 1(a)]. The inner cylinder, made of black Delrin plastic with radius $a=4.49$ cm, is fixed in the present experiment. The outer, with radius $b=5.08$ cm, is made of Duran glass and rotates at angular velocity Ω. The gap between the cylinders is $d=b-a=0.59$ cm, the radius ratio $\eta=a/b=0.883$. Teflon rings are attached to either the inner cylinder or to the inner surface of the outer cylinder a distance $L=53.40$ cm apart, giving an aspect ratio $\Gamma=L/d=90$, large enough to realize a one-dimensional extended system. The working fluid is water or a 28% by weight mixture of glycerol and water with 1% Kalliroscope AQ 1000 added for visualization. The working room temperature is $T=21$ °C, and the kinematic viscosity is $\nu=0.98\times10^{-2}$ cm^2/s for water or $\nu=2.14\times10^{-2}$ cm^2/s for the glycerol-water mixture. The filling level fraction is chosen to be $n=\Theta_f/2\pi=0.75$ (where Θ_f is the angular measure of the azimuthal extent of the fluid), although the particular value does not have a significant influence on the phenomena reported here. Away from the end rings, the base flow state consists of a purely azimuthal flow in the bulk [Fig. 1(b)], recirculation rolls near one free surface, and a boundary-layer-type flow near the other free surface [30]. The bulk flow velocity field consists of two parts: the Couette component, driven by the rotating cylinder pulling fluid around the annulus, and the Poiseuille part driven by the azimuthal pressure gradient necessary to reverse the

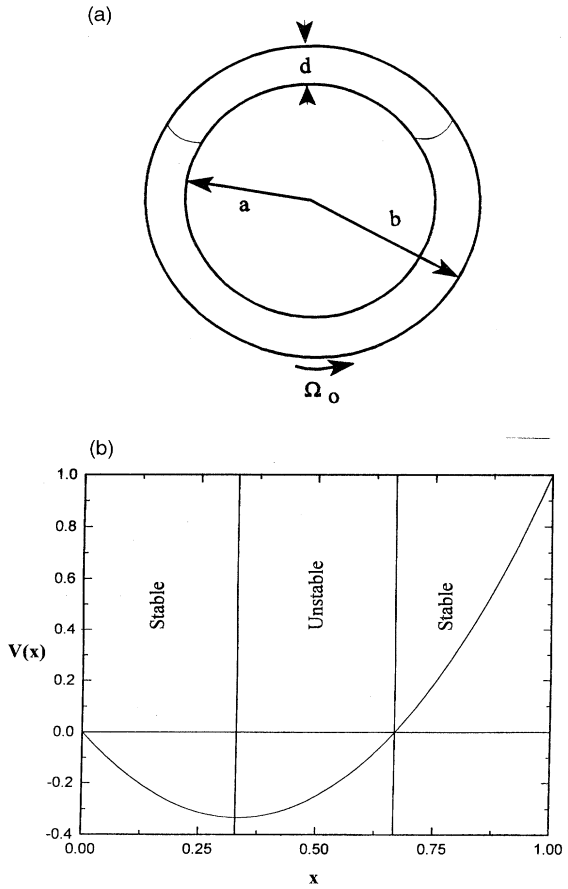

FIG. 1. (a) Geometry of the experimental configuration. (b) Base flow velocity profile far from the free surfaces: $V(x)=x(3x-2)$; the flow has a nodal surface at $x_0=\frac{2}{3}$, and it is potentially centrifugally unstable in the zone $\frac{1}{3}<x<\frac{2}{3}$ and stable elsewhere.

flow at the free surface. The Rayleigh stability criterion applied to the curved streamline flow shows that the Couette component is stable while the Poiseuille part is subject to a Dean centrifugal instability [31]. The recirculation rolls and the boundary-layer flow have azimuthal extensions of about d from the free surfaces. In order to minimize the free surface effects, we chose a relatively small gap in comparison with the mean radius of the system ($d/R\simeq0.1$). Oscillations of the free surfaces induced by gravity may be avoided by rotating the cylinder at reasonably low angular speeds. This has motivated in particular our choice of working fluid solutions with relatively very low viscosity in order to obtain higher values of the control parameter with slow rotation speeds.

We define the control parameter to be the Taylor number with respect to the outer cylinder: $\mathrm{Ta}=R_0(d/R)^{1/2}$, where $R_0=\Omega bd/\nu$ is the outer cylinder Reynolds number. In this work, lengths are scaled by the gap size d, velocities by the diffusion velocity ν/d, and time is scaled by the radial diffusion time $\tau_0=d^2/\nu$. For water $\tau_0=36$ s, and for the glycerol-water mixture $\tau_0=16$ s. To achieve quasistatic conditions and to avoid spurious hysteresis, we have operated

with a time-averaged ramping rate (experimental variation of the outer cylinder Reynolds number between intervals for data collection) $r=dR_0/dt^*\leq 3$, where $t^*=t/\Gamma$. The procedure was to slowly increase R_0, hold it constant for 20 min prior to starting data collection, maintain R_0 constant during data collection (12–20 min), and then resume ramping R_0.

III. EXPERIMENTAL PROCEDURE

A. Space-time diagrams

Spatial dependence data have been obtained using a 28–35 mm variable focal length lens to form an image of the visualized flow on a 1024-pixel charge-coupled device linear array interfaced through a computer-automated measurement and control (CAMAC) system to a computer. The line of 1024 pixels is oriented parallel to the cylinder axis 1 cm below the free surface in the front face. The output consists of intensity maxima and minima which correspond to the centers and boundaries of the rolls. Space-time diagrams are then produced by plotting intensity versus axial position at regular time intervals ($\Delta t=0.14$ s) for different values of the control parameter. The analysis of these plots yields the roll size and other quantities that characterize the evolution of the roll pattern in time and in space with the control parameter. For the analysis of the spatiotemporal intermittency, we have taken data files consisting of 5000 frames, corresponding to a total time of approximately 12 min, which is long enough for accumulating good statistics for the phenomenon under consideration.

B. Binarization of the space-time diagrams

To efficiently extract a useful picture of the behavior in the intermittent state, it is necessary first to identify the turbulent and laminar domains. A binary representation is the simplest approach, and the one usually taken. Binarization of the space-time diagrams makes use of the fast time variation within the turbulent bursts compared with laminar regions. It also emphasizes that the interest is in the burst itself, not the structure of the turbulence. Taking advantage of the latter, the data are first reduced by taking an average of ten space points. This reduces the data set from 1024 pixels in space to 102. The next step is to calculate the second difference in time of the intensity pattern $I''(t)=I(t+2)-2I(t+1)+I(t)$. To determine if a pixel is turbulent, the second difference I'' is compared to the space average of I''. If the difference, $I''-\langle I''\rangle$, is greater than an arbitrary cutoff value, the pixel is said to be turbulent; otherwise it is labeled laminar. This produces a binary space-time diagram of laminar and turbulent regions.

Since the binarization procedure is not perfect, a data massaging routine is then applied. The routine makes use of the fact that a turbulent burst is completely turbulent within its boundaries in space and time; i.e., there should not be laminar pixels inside a turbulent burst. Also, the turbulent bursts are of a finite size, and spurious turbulent pixels must be removed. To implement this, the routine's first step is to check if each turbulent pixel has two or more turbulent neighbors out of the eight nearest neighbors in space and time. If it does, it remains turbulent. If it does not, it is switched to laminar. In a second pass over the data, if any laminar pixel has three or more turbulent neighbors, it is switched to turbulent. A third pass is similar to the first, except that a turbulent pixel must now have three or more neighbors to remain turbulent. During the next pass over the data, if the ith pixel is turbulent and the $i+5$ (in space) pixel is turbulent, all pixels in between are also considered turbulent. The fifth pass involves the same procedure, except it checks the fifth pixel away in time and the last pass checks the fifth pixel in space again. This routine is designed to remove spurious turbulent pixels and to fill in gaps in the turbulent domains that are not real.

Variations of this routine have been used with different nearest neighbor requirements, and different massaging lengths. A comparison with the raw data shows that the procedure is insensitive to the parameter variations when applied with a corresponding slight adjustment of the cutoff value. In addition, the procedure, as described above, is applied with numerous cutoff values. The binarized output then is compared with the raw data to ensure its accuracy.

The binary representation allows us to measure the main characteristics (order parameter, statistics, etc.) of the spatiotemporal intermittency.

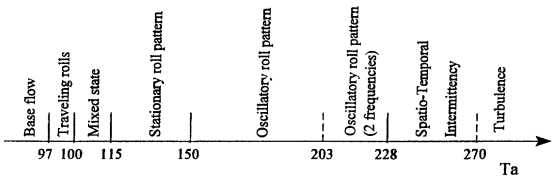

FIG. 2. Diagram of the different states observed in the Taylor-Dean system when the inner cylinder is fixed.

IV. EXPERIMENTAL RESULTS

A. Sequence of states

The sequence of the states observed in the system is given in Fig. 2. The first roll pattern occurs in the form of traveling inclined rolls at approximately Ta=97. These rolls appear near the recirculation zone, and their axial extent grows with the control parameter until they fill the whole system [Fig. 3(a)]. The transition does not show any hysteresis when ramping up and down, within our resolution of 1%. The drift velocity $v_d=27$, and the wavelength of the pattern is $\lambda=1.170$.

For Ta$\in$[100,115[, the pattern is a mixed state of traveling rolls superimposed on a stationary roll pattern with different wavelengths λ_1 and λ_2 [Fig. 3(b)]. Such a state has also been observed recently in experiments in the Taylor-Couette system with axial flow [32].

For Ta=115, the mixed state becomes stationary. This transition is subcritical and highly hysteretic. It is characterized by the existence of a front separating the disappearing chaotic state and the emerging almost stationary roll pattern. The space-time plot exhibits an asymmetric roll pattern where large and small rolls alternate in a chaotic way, giving rise to mean wavelengths in a ratio $\frac{2}{3}$ [Fig. 3(c)].

The stationary roll pattern becomes unstable to monoperiodic oscillations for Ta$\in$[150,203[[Fig. 3(d)], followed by biperiodic oscillations for Ta$\in$[203,225[. The biperiodic oscillations are characterized by two different frequencies; the

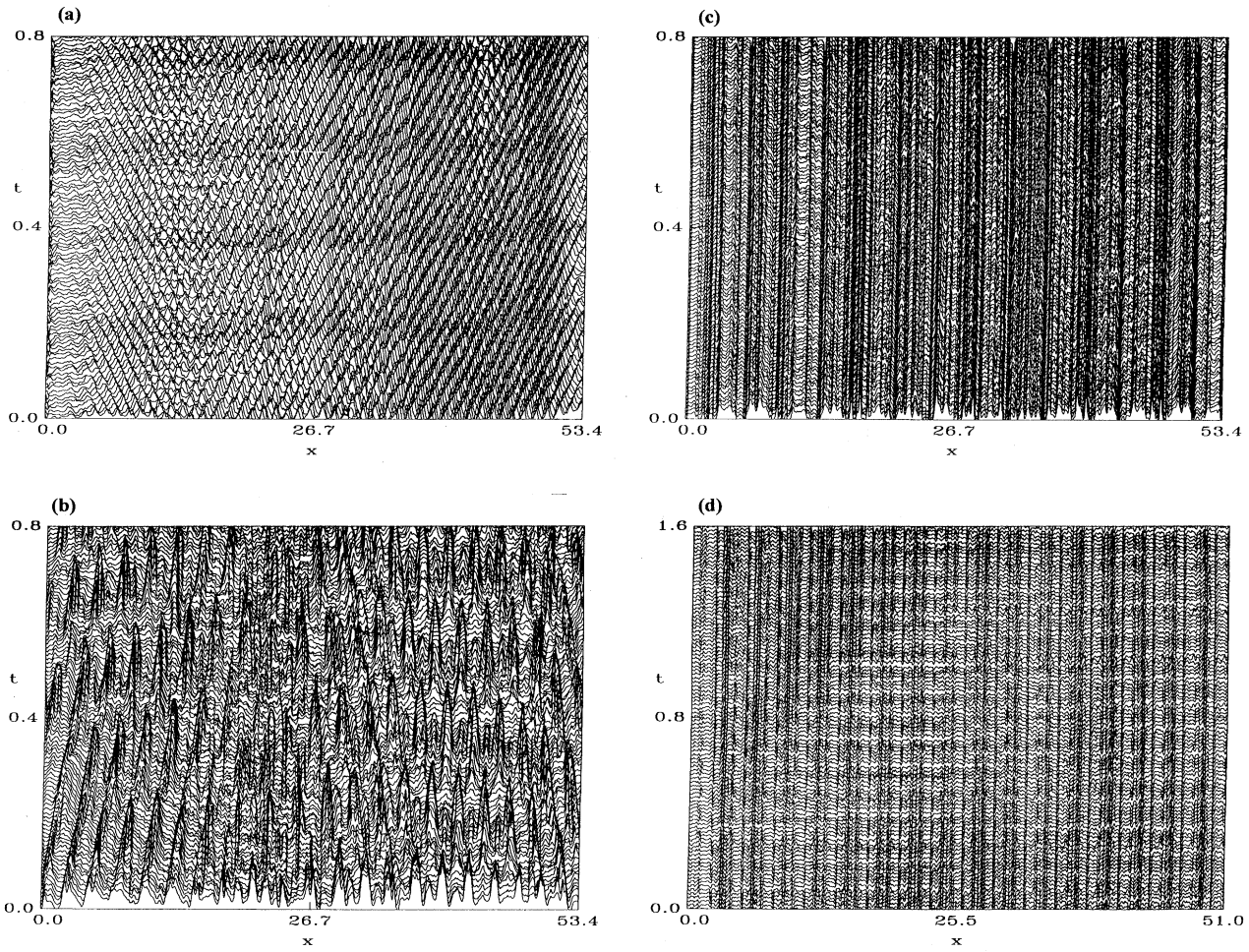

FIG. 3. Space-time diagrams of the different states observed in the Taylor-Dean system before weak turbulence sets in: (a) Traveling rolls pattern for Ta=100. (b) Mixed state of traveling and stationary rolls for Ta=111. (c) Stationary roll pattern for Ta=115. (d) Oscillatory roll pattern for Ta=174.

first oscillation frequency corresponds to a wavy-vortex-like instability, while the second frequency corresponds to a modulational type instability. It has been observed in particular that the oscillations occur between two neighboring rolls inside the large wavelength, and have properties that are similar to a collective mode with fixed nodes.

Upon a further increase of the control parameter, the oscillating pattern exhibits a continuous nucleation of spatiotemporal defects (collisions at some space positions and roll generation at others) which already reduce the correlation length of the pattern and induce a chaotic behavior. These spatiotemporal defects generate turbulent bursts in our system which last a short time before disappearing from the flow pattern. For larger values of the control parameter, the spatiotemporal intermittency is sustained and the typical size of laminar domains decreases.

The regime beyond the spatiotemporal regime is very turbulent, and it has not been characterized by the available experimental tools. It should just be mentioned that the flow exhibits some underlying spatially coherent rolls with a mean wavelength comparable to the large wavelength of the stationary pattern.

B. Spatiotemporal intermittency

The spatiotemporal intermittent regime is characterized by the coexistence of a spatially ordered pattern with turbulent patches or bursts which appear irregularly in time and in different positions [Figs. 4(a)–4(c)]. Using an analogy with thermodynamics, the spatiotemporal intermittency can be considered as a two-phase state with one phase stable and the other metastable. The first turbulent bursts result from the Eckhaus-type instability when rolls collide or are generated. This process forces the pattern to adjust its wavelength and to nucleate localized perturbations which will be driven away in the azimuthal direction. These bursts occur spontaneously, do not propagate into the neighboring laminar state, and decay rapidly. For higher rotation rates of the cylinder, the turbulent bursts grow in time, and in size, by propagating into neighboring laminar domains. The turbulence spreads in this regime: the size of laminar domains diminishes as the control parameter increases, giving rise to an almost completely turbulent state. Therefore, we distinguish two dynamic types of turbulent bursts: localized turbulent patches resulting from the nucleation of defects, and active turbulent bursts which tend to destroy laminar domains.

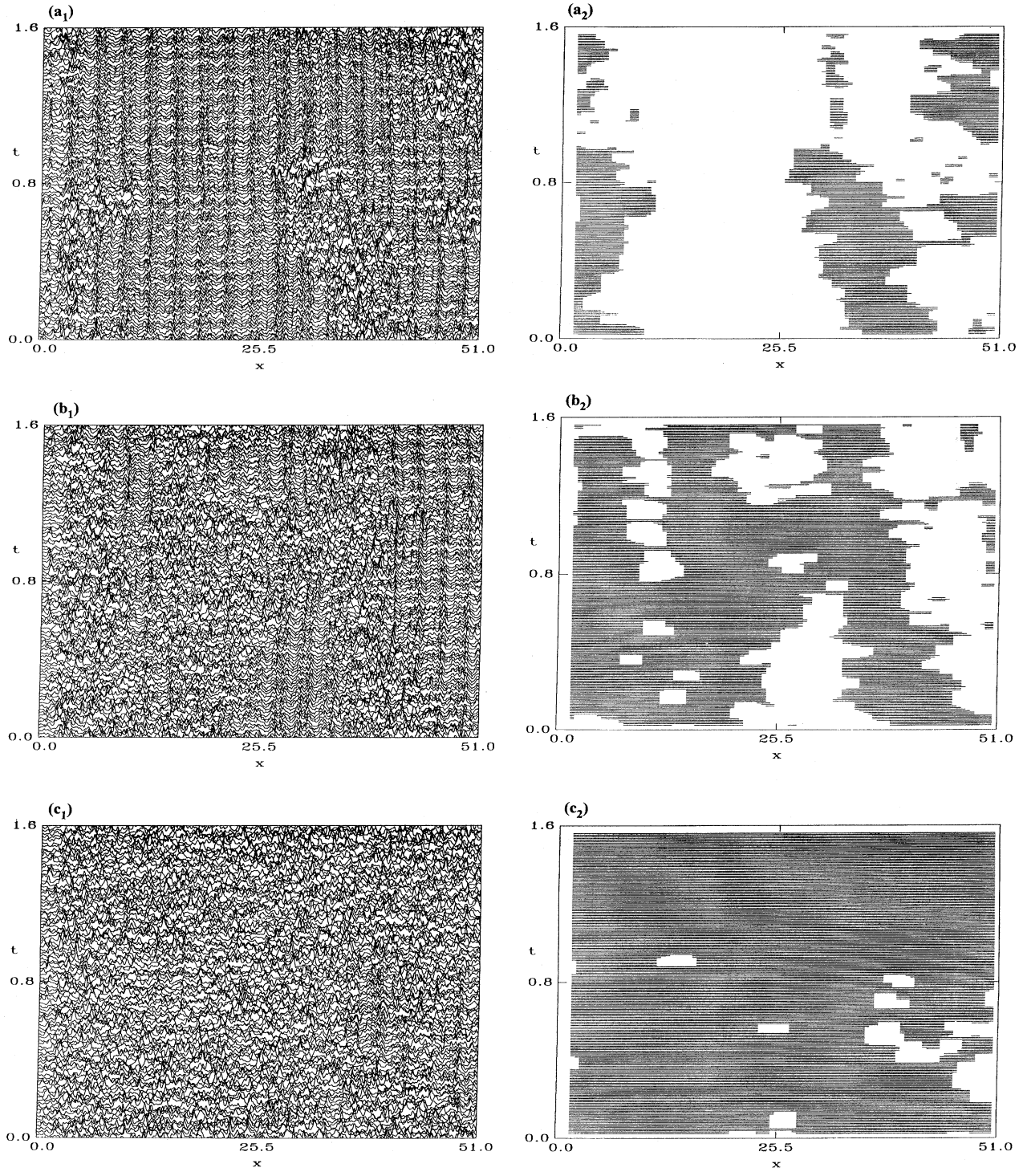

FIG. 4. Space-time diagrams of the patterns and their binarized versions in the spatiotemporal regime: (a) Ta=235 above the onset of the STI; the pattern contains few turbulent domains. (b) Ta=240 above the onset of the exponential regime; the turbulent zones and laminar domains in the pattern have approximately the same average size. (c) Ta=254; the pattern contains few laminar domains.

Behavior of the turbulent fraction

Using the binarization procedure on the space-time diagrams of the flow pattern as described in Sec. II, we have represented in black the turbulent domains and in white the laminar ones. This representation allows us to easily measure the *time-averaged spatial turbulent fraction* (referred to simply as the turbulent fraction f) as well as the *temporal turbulent fraction* (called also the *intermittency factor* γ) which

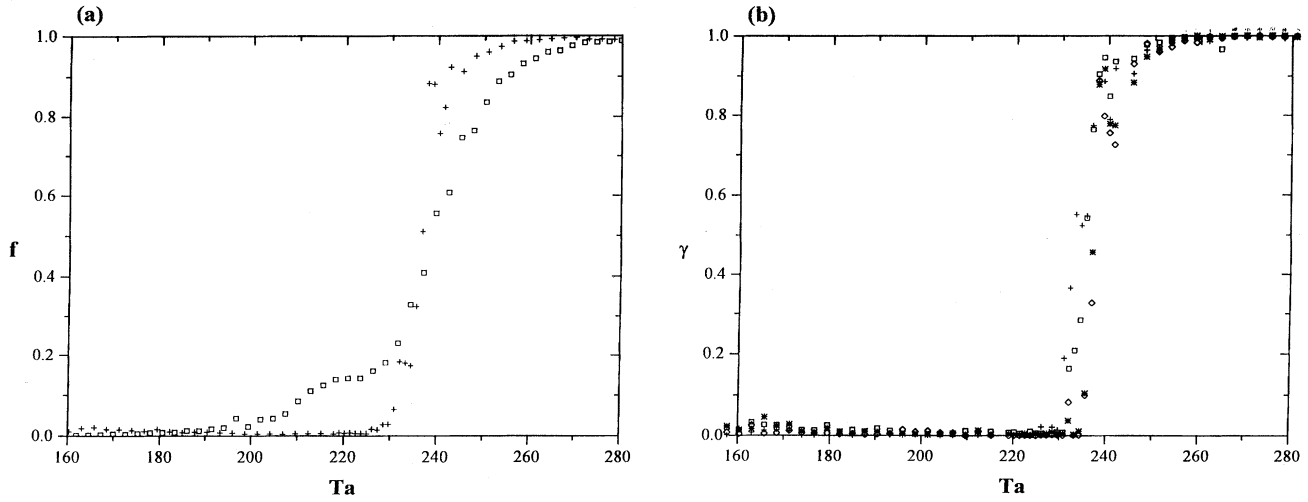

FIG. 5. (a) Spatial turbulent fraction as a function of the control parameter; the crosses (+) correspond to the case when the end rings are attached to the inner cylinder, the squares (□) to the case when the end rings rotate with the outer cylinder. In the latter case, the imperfect nature of the bifurcation comes from the Ekman cells, which induce a localized turbulence to the ends before the onset of spatiotemporal intermittency in the bulk flow. (b) Intermittency factor measured at different positions (+) at $x=8.7$, (□) at $x=16.8$, (*) at $x=29.1$, and (◇) at $x=38.3$.

are, respectively, the ratio of the total area of turbulent patches to the total area of the space-time diagram and the ratio of the mean duration of turbulent patches to the total measurement time. The turbulent fraction plays the role of the order parameter in this problem, and varies with the control parameter Ta [Figs. 5(a)–5(c)]. The behavior of the turbulent fraction depends on the boundary conditions imposed on the flow: whether the end rings are attached to the inner cylinder or rotate with the outer cylinder affects the details of the transition process.

When the rings are attached to the fixed inner cylinder, the transition to spatiotemporal intermittency occurs via a perfect bifurcation with a definite onset. The spatial turbulent fraction exhibits a net threshold at $\mathrm{Ta}_0=228\pm1$, indicating the transition to spatiotemporal intermittency [Fig. 5(a)]. Near the onset of the STI, the turbulent fraction grows as a power law with the control parameter, i.e., $f(\mathrm{Ta})=f_0[(\mathrm{Ta}-\mathrm{Ta}_0)/\mathrm{Ta}_0]^{\beta}$, where the exponent $\beta=1.30\pm0.26$. The intermittency factor, i.e., the temporal turbulent fraction measured at different spatial locations, shows also a net transition with a similar linear behavior [Fig. 5(b)].

When the rings are attached to the rotating outer cylinder, they induce Ekman cells which create turbulence near the ends for $\mathrm{Ta}\geqslant190$. This end region turbulence forces the oscillatory Dean rolls and induces localized turbulent bursts. In that case, the transition to spatiotemporal intermittency is slightly modified and becomes imperfect. Therefore, for $\mathrm{Ta}<\mathrm{Ta}_0$, turbulent bursts already occur in the flow, while at $\mathrm{Ta}=\mathrm{Ta}_0$, the turbulent fraction has grown to approximately 10% [Fig. 5(a)]. We have measured the different parameters for this regime, and have found that besides the imperfect nature of the transition and the slope of the curves $f(\mathrm{Ta})$, the other characteristics were less modified by the end turbulence. Therefore, STI is a robust property of the flow, and the imperfection has a real impact only on details of the transition.

The power spectrum of the spatiotemporal regime is characterized by a broadband background. The noise fraction f_N, defined as the ratio of the area covered by the broadband background A_b to the total area A of the spatial power spectrum, is approximately the same as the turbulent fraction measured from the binarized plots (Fig. 6). Thus the noise fraction represents a precise measure of the turbulent fraction since it does not depend on an arbitrary imposed cutoff.

Laminar and turbulent domains distribution

We have examined the statistics of the laminar (white) and turbulent (black) domains by analyzing the distribution of the domains with their length (Fig. 7). For control parameter values close to the onset of the spatiotemporal intermittency, the distribution of the laminar domains may be represented by a power law $N(l)\sim l^{-\mu}$ (algebraic decay) over a

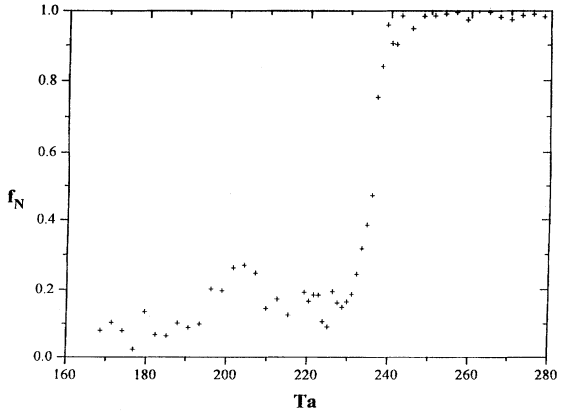

FIG. 6. Noise background fraction as an alternative measure of the turbulent fraction.

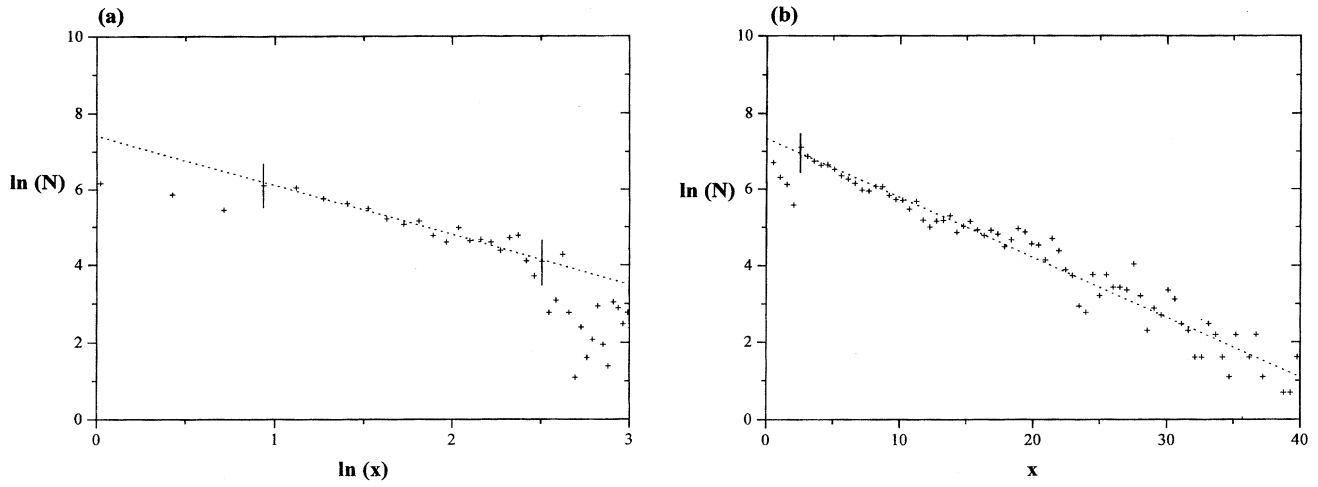

FIG. 7. Histograms of the laminar domains: (a) In the algebraic regime (Ta=233). (b) In the exponential regime (Ta=237).

factor of 5 range in domain size, somewhat smaller than found in other experiments on STI [23]. We have found that, for three separate values of the cutoff, the exponent $\mu=1.7 \pm 0.1$ for Ta$\in$[228,234]. It should be noted that domains smaller than $\ln x=1$ represent laminar structures of the order of the roll size and smaller. As previously discussed, the internal structure of the turbulent bursts is outside the scope of this work, and therefore the small domains will not be included in the fits. Furthermore, the longer domains in the histograms of the algebraic regime exhibit some exponential falloff reminiscent of the crossover regime found in Rayleigh-Bénard convection [23]. For Ta$\geqslant$235, the histograms cannot be fit by a power law. For Ta$\in$[237,270[, the distribution of the laminar domains with their size exhibits an exponential law $N(l)\sim e^{-ml}$ (exponential decay). The quantity $1/m=l_c$ is the characteristic width of the laminar domains. It decreases with the control parameter with the dependence $l_c(\mathrm{Ta})=l_0(\mathrm{Ta}-\mathrm{Ta}_c)^{-\alpha}$, where $\alpha=0.64$ [Fig. 8(a)], meaning that the scales of the laminar domains are becoming small rapidly in the exponential regime. The value $\mathrm{Ta}_c=237$ was chosen to be the threshold of the second transition in the spatiotemporal intermittency: below this value, the turbulent domains are embedded in a laminar background, and, above it, the laminar zones are embedded in a turbulent background. The distribution of the turbulent domains exhibits only an exponential regime $N(l)=N_0e^{-l/l_t}$, where l_t is the characteristic width of the turbulent bursts. Their characteristic width l_t increases with the control parameter [Fig. 8(b)].

The temporal histograms show similar behavior, in particular, the algebraic regime and exponential regimes are seen: the power law gives an exponent $\mu_t=1.7$ for Ta$\in$[228,237[, and the characteristic time (lifetime) of the laminar domains decreases with the control parameter after

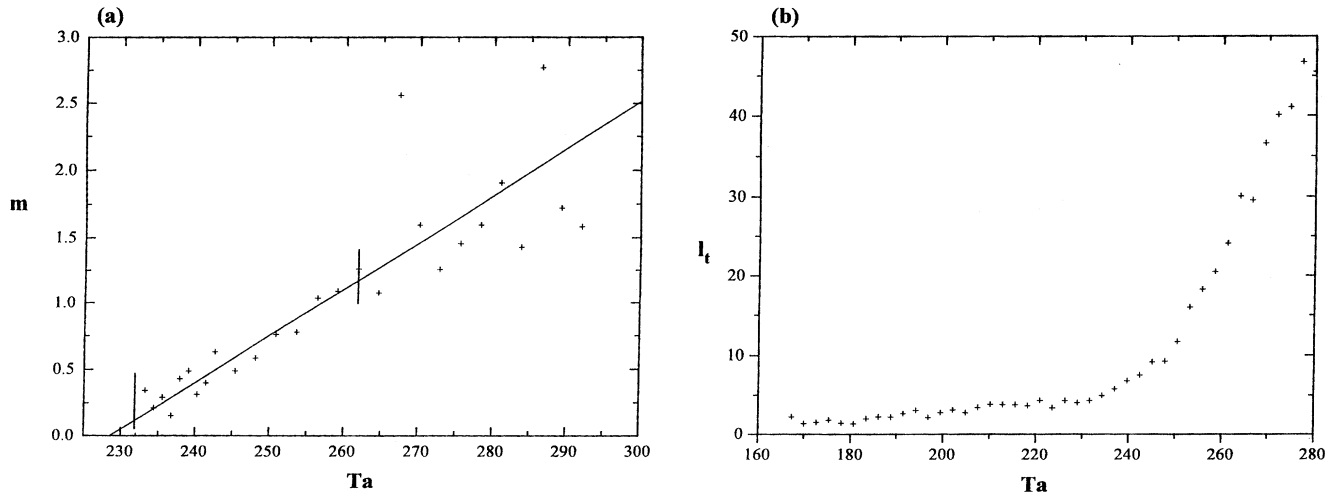

FIG. 8. (a) Inverse of the characteristic width of the laminar domains in the exponential regime. (b) Characteristic width of the turbulent domains in the spatiotemporal regime (with rotating end rings).

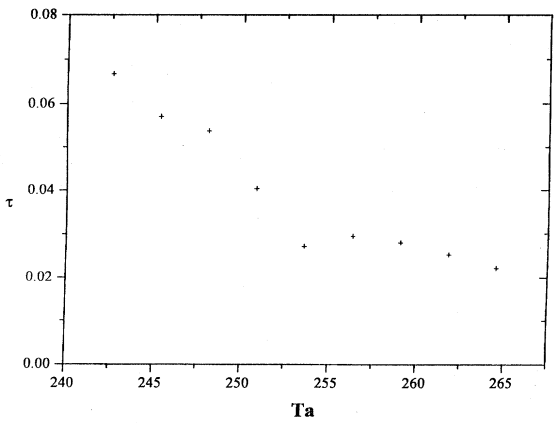

FIG. 9. Lifetime of laminar domains as a function of the control parameter.

the law: $m_t \sim (\mathrm{Ta}-237)^{-\alpha_t}$, where $\alpha_t=0.73$. The lifetime of the turbulent domains grows with the control parameter (Fig. 9).

Correlation function and length

To complete the statistical analysis of the spatiotemporal intermittency in the Taylor-Dean system, we have computed the correlation function and correlation length of the laminar and turbulent domains for binarized space-time plots. The correlation function is defined as

$$C(x)=\frac{\langle [I(z+x,t)][I(z,t)]\rangle}{\langle I(z,t)^2\rangle}, \tag{1}$$

where $I(z,t)=0$ or 1. Below the transition, we assign 1 to turbulent domains and 0 to laminar, and the reverse above the transition. This approach makes clear that we are calculating correlations of the fluctuations on a background state. Below Ta_c, turbulent domains are a fluctuation on a laminar background, and *vice versa* above Ta_c. This method of calculating the correlation function is borrowed from the study of spin lattices [33]. From the resulting correlation function [Fig. 10(a)], we have calculated the correlation length separately for both laminar and turbulent domains. The obtained correlation lengths diverge near $\mathrm{Ta}_c=237$ [Fig. 10(b)], showing that there is a separation between two distinct regimes: for $\mathrm{Ta}<\mathrm{Ta}_c$ the correlation length of the turbulent domains grows and becomes infinite at Ta=237, while for Ta>237 the correlation length of the laminar regions decreases. Therefore, the correlation length divergence can be considered as the hallmark of the critical point corresponding to the transition to the exponential regime. The behavior of the correlation length near Ta_c can be represented as follows:

$$\xi \sim \begin{cases} (\mathrm{Ta}-\mathrm{Ta}_c)^{-\nu} & \text{for } \mathrm{Ta}>\mathrm{Ta}_c \\ (\mathrm{Ta}_c-\mathrm{Ta})^{-\nu'} & \text{for } \mathrm{Ta}<\mathrm{Ta}_c . \end{cases} \tag{2}$$

The best fit gives the following values of the critical exponents for the correlation length: $\nu \simeq 0.53$, and $\nu' \simeq 1.20$. Therefore, for $\mathrm{Ta}<\mathrm{Ta}_c$, the turbulent domains are the fluctuations developing in a laminar background, while for $\mathrm{Ta}>\mathrm{Ta}_c$ the laminar zones are the fluctuations dying in the turbulent background. The difference between ν and ν' might be attributed to the difference in the nature of the turbulent bursts below and above Ta_c. The correlation length measured that way is approximately the same as that obtained from the raw space-time diagrams. The coherence time of laminar and turbulent domains has been computed in the same way and it shows similar behavior, in particular a divergence near the threshold Ta_c of the exponential regime.

V. DISCUSSION OF THE RESULTS

A. Spatiotemporal intermittency in other systems

The spatiotemporal intermittency in the Taylor-Dean system exhibits two regimes with two threshold values: the first corresponds to an algebraic regime with a threshold $\mathrm{Ta}_a=228$, and the second regime is exponential with a threshold at $\mathrm{Ta}_c=237$. For Ta<237, the turbulent bursts (metastable phase) nucleate spontaneously, and they are localized in space and time. The characteristic width of the laminar domains is infinite, i.e., approximately the same as

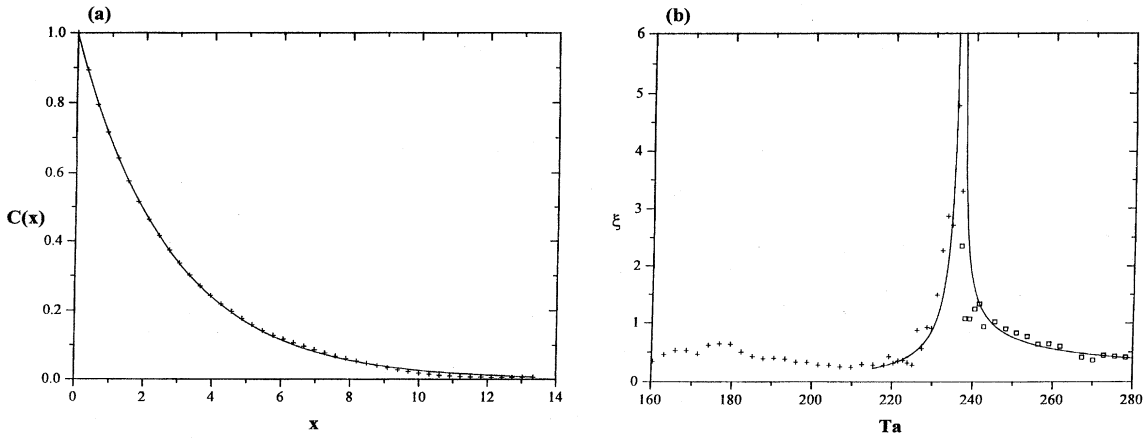

FIG. 10. (a) Correlation function of the binarized space-time plot (Ta=233); measured points (+) are shown, along with a solid line representing the exponential fit $C(x)=Ae^{-x/\xi}$, where $A=0.995$ and $\xi=2.786$. (b) The correlation length ξ divergence near the critical point.

TABLE I. Experimental values of different exponents measured in systems exhibiting spatiotemporal intermittency.

Experimental System	β	μ_s	μ_t	α_s	α_t	ν	ν'
Convection in annulus [23]		1.9±0.1	1.9	0.5			
Convection in channel [20]	0.3±0.05	1.6±0.2	2.0±0.2	0.50±0.05	0.50±0.05		
Convection in annulus [20]		1.7±0.1	2.0±0.1	~0.50	~0.50		
Roll coating system [24]	0.45±0.05	0.63±0.02	0.61±0.02	0.50	0.50		
Taylor-Dean system	1.30±0.26	1.67±0.14	1.74±0.16	≃0.64	≃0.73	≃0.53	1.20

the length of the whole system. For Ta>237, the turbulent bursts (stable phase) form a connected pattern with an embedding of laminar zones (metastable phase) whose characteristic width decreases significantly with Ta to a few wavelengths of the initial pattern. The correlation length of the laminar and turbulent domains diverge near the value $Ta_c=237$, which is considered the critical point corresponding to the onset of the exponential regime. (In a recent experimental study of the capillary ripples [11], the divergence of the correlation time has been used to determine the onset of the *order-disorder* transition.)

In connection with Pomeau's conjecture, the value $Ta_c=237$ corresponds to a critical point for a second-order phase transition. However, the critical exponents measured in our experiment (β,α,ν,ν') are different from those predicted by theories of critical phenomena (Landau mean field theory [33], directed percolation theory [34], etc.). The spatiotemporal intermittency observed in other one-dimensional extended systems exhibits two distinct regimes (algebraic and exponential), but the exponents characterizing each regime and the turbulent fraction differ from one experiment to another. In Table I we give values of different exponents from various experiments. The differences originate apparently in the behavior of the laminar background flow pattern on which the spatiotemporal intermittency sets in. In some cases, there are localized bursts, as in Rayleigh-Bénard convection [23], or in the Taylor-Dean system, while in the printer's instability there are dilation waves which may explain the difference in the coefficients. Therefore, it is unlikely that all reported experiments belong to the same class of STI universality even though they exhibit the main features of Pomeau's conjecture. It is worthwhile to notice that the different numerical simulations on partial differential equations ([19],[20]), on coupled map lattices [18] and on cellular automata [22] have also shown spatiotemporal intermittency with different exponents.

B. Physical origin of STI in the Taylor-Dean system

The question of the physical origin of the spatiotemporal intermittency in dimensional systems remains open. In the Taylor-Dean system, there are two plausible causes of the STI: a self-excitation mode from the recirculation zone in the front surface, and the secondary instability of the longitudinal rolls.

Theoretical investigation and numerical simulations of the recirculation zone [30] indicates that in the front face there exists an oscillating recirculation roll aligned parallel with the cylinder axis, with a frequency growing with the control parameter. We therefore have a system with a natural frequency and with a source oscillating at a frequency depending on the control parameter. Such systems give rise to the so-called *parametric instability* and, after the Mathieu equation theory, their solutions can be described by tonguelike curves near the resonance in a convenient parameter space [35]. Therefore, a resonance mechanism could be at the origin of the different states observed in this system, the STI occuring in the tonguelike domain at large amplitude.

The STI could also be induced by the shear instability of the mean flow, as has been suggested by recent studies [36]. In fact, the base flow consists of Poiseuille and Couette parts separated by a nodal surface [31]. The first instability gives rise to streamwise vortices which should be subject to a secondary instability of traveling waves due to the shear instability of the nodal surface. The growth of this secondary instability can trigger the sudden occurrence of turbulent fluctuations in the bulk flow. Recent experimental studies have shown that the intermittency can occur at Re~400 in the plane Couette flow [37,38], while it occurs at Re~1000 in the plane Poiseuille flow [16]. We use the latter value to estimate the critical Taylor number for intermittency in the Taylor-Dean system (since the Poiseuille part is the largest of the base flow) and we find that $Ta^*=Re^*\ (h/R)^{1/2}=279$, where $h=2d/3$ is the width of the Poiseuille part of the base flow (this value is 15% higher than the observed threshold of STI). The existence of the Dean rolls and of the Couette flow might lower this value. However, no firm conclusion can be made before an extensive study is performed on the Poiseuille flow with the velocity profile of Fig. 1 in order to confirm this mechanism.

VI. CONCLUSION

The spatiotemporal intermittency observed in a Taylor-Dean system with the inner cylinder fixed has been investigated. The main parameters characterizing this transition scenario have been computed from experimental data. The STI exhibits two different dynamical regimes (algebraic and ex-

ponential). Near the onset of the exponential regime, the correlation length and correlation time of domains diverge. This behavior calls for an analogy of this transition with second-order phase transitions in equilibrium systems. The measured exponents in the Taylor-Dean system differ from those obtained in other recently reported experiments, which raises again the question of the universality of spatiotemporal intermittency. The physical origin of spatiotemporal intermittency remains an open question which necessitates further investigation.

ACKNOWLEDGMENTS

The authors acknowledge fruitful discussions with P. Manneville, C. Jayaprakash, B. Patton, and P. Colovas. The project is supported partly by DRET and NATO.

[1] P. Manneville, *Dissipative Structures and Weak Turbulence* (Academic, New York, 1990).
[2] B. Castaing, G. Gunaratne, F. Heslot, L. Kadanoff, A. Libchaber, S. Thomae, X. Z. Wu, S. Zaleski, and G. Zanetti, J. Fluid Mech. **204**, 1 (1989).
[3] C. Meneveau and K. R. Sreenivasan, J. Fluid Mech. **224**, 429 (1991).
[4] *Turbulence: A Tentative Dictionary, Vol. 341 of NATO Advanced Study Institute, Series B: Physics*, edited by P. Tabeling and O. Cardoso (Plenum, New York, 1995). See, in particular, the contributions by F. Daviaud and by H. Chaté and P. Manneville.
[5] L. D. Landau and E. M. Lifshitz, *Fluid Mechanics* (Pergamon, New York, 1987).
[6] M. Cross and P. C. Hohenberg, Rev. Mod. Phys. **65**, 851 (1993).
[7] P. Bergé, Nucl. Phys. B **2**, 247 (1987).
[8] C. D. Andereck, S. S. Liu, and H. Swinney, J. Fluid Mech. **164**, 155 (1986).
[9] I. Mutabazi, J. J. Hegseth, C. D. Andereck, and J. E. Wesfreid, Phys. Rev. Lett. **64**, 1729 (1990). See also I. Mutabazi and C. D. Andereck, *ibid.* **70**, 1429 (1993).
[10] M. Rabaud, S. Michalland, and Y. Couder, Phys. Rev. Lett. **64**, 184 (1990).
[11] N. B. Tufillaro, R. Ramshankar, and J. P. Gollub, Phys. Rev. Lett. **62**, 422 (1989).
[12] B. J. Gluckman, P. Marcq, and J. P. Gollub, Phys. Rev. Lett. **71**, 2034 (1993).
[13] D. J. Tritton, *Physical Fluid Dynamics* (Oxford University Press, Oxford, 1989).
[14] I. J. Wygnanski and F. H. Champagne, J. Fluid Mech. **59**, 281 (1973). A recent experiment is reported by D. Stassinopoulos, J. Zhang, P. Alstrom, and M. T. Levinsen, Phys. Rev. E **50**, 1189 (1994).
[15] D. R. Carlson, S. E. Widnall and M. F. Peeters, J. Fluid Mech. **121**, 487 (1982).
[16] M. Nishioka and M. Asai, J. Fluid Mech. **150**, 441 (1985).
[17] D. Coles, J. Fluid Mech. **21**, 385 (1965).
[18] K. Kaneko, Prog. Theor. Phys. **74**, 1033 (1985). See also H. Chaté and P. Manneville, Physica D **32**, 409 (1988); Europhys. Lett. **6**, 591 (1988). See also J. R. de Bruyn and L. Pan, Phys. Rev. E **47**, 4575 (1993).
[19] H. Chaté and P. Manneville, Phys. Rev. Lett. **58**, 112 (1987).
[20] F. Daviaud, J. Lega, P. Bergé, P. Coullet, and M. Dubois, Physica D **55**, 287 (1992). See also H. Chaté, Nonlinearity **7**, 185 (1994).
[21] R. J. Deissler, J. Stat. Phys. **40**, 371 (1985).
[22] H. Chaté and P. Manneville, Europhys. Lett. **6**, 591 (1988). See also H. Chaté and P. Manneville, J. Stat. Phys. **56**, 357 (1989).
[23] S. Ciliberto and P. Bigazzi, Phys. Rev. Lett. **60**, 286 (1988). See also F. Daviaud, M. Bonetti, and M. Dubois, Phys. Rev. A **42**, 3388 (1990).
[24] M. Rabaud and S. Michalland, Physica D **61**, 197 (1992). See also S. Michalland, M. Rabaud, and Y. Couder, Europhys. Lett. **22**, 17 (1993). See also M. Decré. E. Gailly, J.-M. Buchlin, and M. Rabaud, in *Spatio-Temporal Patterns in Nonequilibrium Complex Systems*, edited by P. E. Cladis and P. Palffy-Muhoray (Addison-Wesley, Reading, MA, 1994).
[25] E. Bosch and W. van de Water, Phys. Rev. Lett. **70**, 3420 (1993).
[26] H. Willaime, O. Cardoso, and P. Tabeling, Phys. Rev. E **48**, 288 (1993).
[27] Y. Pomeau, Physica D **23**, 3 (1986).
[28] P. Grassberger and T. Schreiber, Physica D **50**, 177 (1991); D. Stassinopoulos and P. Alstrom, Phys. Rev. A **45**, 675 (1992).
[29] I. Mutabazi and C. D. Andereck, Phys. Rev. A **44**, R6169 (1991).
[30] C. Normand, I. Mutabazi and J. E. Wesfreid, Eur. J. Mech. B **10**, 335 (1991). See also K. S. Chen, A. C. Ku, T. M. Chan, and S. Z. Yang, J. Fluid Mech. **213**, 149 (1990).
[31] I. Mutabazi, C. Normand, H. Peerhossaini, and J. E. Wesfreid, Phys. Rev. A **39**, 763 (1989).
[32] A. Tzameret and V. Steinberg, Phys. Rev. E **49**, 4077 (1994).
[33] R. J. Baxter, *Exactly Solved Models in Statistical Mechanics* (Academic, New York, 1982).
[34] S. P. Oboukhov, Physica A **101**, 145 (1984).
[35] E. Meron, Phys. Rev. A **35**, 4892 (1987).
[36] K. Coughlin and P. S. Marcus (unpublished); To appear in "Boundaries, Interfaces and Transitions," Proceedings of the 1995 CRM Summer School, Banff, Canada (AMS, 1996). See also K. Coughlin (unpublished).
[37] J. Hegseth, F. Daviaud, and P. Bergé, in *Ordered and Turbulent Patterns in Taylor-Couette Flow*, edited by C. D. Andereck and F. Hayot (Plenum, New York, 1992).
[38] O. Dauchot, These de doctorat, Université Paris 6, 1995.